Journal of Solid State Chemistry 184 (2011) 2588–2594

Contents lists available at ScienceDirect

Journal of Solid State Chemistry

journal homepage: www.elsevier.com/locate/jssc

Oxygen excess in the "114" cobaltite hexagonal structure: The ferrimagnet $CaBaCo_4O_{7.50}$

V. Pralong*, V. Caignaert, T. Sarkar, O.I. Lebedev, V. Duffort, B. Raveau

Laboratoire CRISMAT, UMR 6508 CNRS ENSICAEN, 6 bd Maréchal Juin, 14050 Caen, France

ARTICLE INFO

Article history:
Received 18 April 2011
Received in revised form
12 July 2011
Accepted 23 July 2011
Available online 2 August 2011

Keywords:
114
Cobaltite
$CaBaCo_4O_7$
Oxidation
Peroxo group
Ferrimagnetism

ABSTRACT

The study of the oxidation of the "114" orthorhombic cobaltite $CaBaCo_4O_7$, using first electrochemistry and then soft chemistry based on oxidation by NaClO, has allowed a new phase, $CaBaCo_4O_{7.50}$, to be prepared topotactically. The structural study of this phase shows that its hexagonal structure, closely related to that of orthorhombic $CaBaCo_4O_7$, is curiously similar to that of the members of the $LnBaCo_4O_7$ series, in spite of its excess oxygen. Its magnetic study shows that this phase, like $CaBaCo_4O_7$, is ferrimagnetic with the same T_C (60 K), but differently exhibits an unusual magnetic hysteresis. This exceptional behavior of $CaBaCo_4O_7$ with respect to oxidation as well as the magnetic properties of $CaBaCo_4O_{7.50}$ is interpreted in terms of the presence of defects due to oxidation.

© 2011 Elsevier Inc. All rights reserved.

1. Introduction

Cobaltites with the generic formulation $LnBaCo_4O_7$ (*Ln*: lanthanide, Y), discovered some years ago [1,2], represent a new class of oxides that is studied as a model system by many researchers for both, its complex crystal chemistry and magnetic properties. From the structural viewpoint, this oxide family is closely related to that of spinels, since like the latter, it consists of the stacking of triangular and kagome layers of cobalt polyhedra, generated by a close packing of oxygen atoms, so that, ferrites with a similar structure were recently synthesized [3]. Nevertheless, in contrast to spinels, the cobalt ions of the kagomé layers do not exhibit the octahedral coordination, but the tetrahedral one. Moreover, these compounds exhibit a structural transition from a hexagonal ($P6_3mc$) or trigonal ($P31c$) symmetry to an orthorhombic symmetry ($Pbn2_1$) as the temperature is decreased, the transition temperature varying with the size of the Ln^{3+} cation from 313 K for Y to 175 K for Yb [4–6]. The magnetic properties of this class of oxides are dominated by the particular triangular geometry of the Co–O framework, so that magnetic frustration is in competition with magnetic ordering, leading to complex magnetic transitions as exemplified by the cobaltite $YBaCo_4O_7$. The latter was first reported to exhibit a spin glass transition around $T_{sg}\sim 66$ K [7], whereas long range magnetic order was evidenced below $T_N=110$ K [4] and a magnetic transition, with short range correlations, was revealed above T_N [8] for this phase. The interest for the "114" system has been recently stimulated by the discovery of the $CaBaCo_4O_7$ cobaltite, which is different from all other members of the series, exhibits complex ferrimagnetic ordering below $T_C=70$ K and charge ordering in a wide temperature range from 4 K to room temperature [9,10].

In addition to their remarkable physical properties, the "114" cobaltites have been shown to exhibit extraordinary ability for oxygen absorption and mobility. The great affinity of these compounds for oxygen was first demonstrated for $YBaCo_4O_7$ [11,12], whereas the reversibility of the phenomenon and the oxygen storage capability, up to 1.40 O per formula, was then shown for the $LnBaCo_4O_{7+\delta}$ series [13]. First determined for $YBaCo_4O_{8.1}$ [14], the distribution of oxygen atoms appears very complex in the whole series $YBaCo_4O_{7+\delta}$ [15], depending on the δ value and is so far not understood. Bearing in mind these results, we have considered the possibility of oxidation of the orthorhombic structure of $CaBaCo_4O_7$. We report herein on a novel cobaltite $CaBaCo_4O_{7.50}$ synthesized from the pristine orthorhombic form $CaBaCo_4O_7$, by electrochemical reaction and by soft chemistry. We show that, unlike $CaBaCo_4O_7$, this new phase exhibits the hexagonal symmetry, similar to $YBaCo_4O_7$. Moreover it is observed that $CaBaCo_4O_{7.5}$ is, like $CaBaFe_4O_7$, ferrimagnetic, but with a lower value of the Curie temperature ($T_C=60$ K) and exhibits a very different hysteresis loop, indicating a soft ferrimagnetic behavior. This extraordinary presence of oxygen excess in the hexagonal matrix is discussed.

* Corresponding author. Fax: +33 2 31 95 16 00.
E-mail address: valerie.pralong@ensicaen.fr (V. Pralong).

0022-4596/$ - see front matter © 2011 Elsevier Inc. All rights reserved.
doi:10.1016/j.jssc.2011.07.039

2. Experimental section

2.1. Synthesis of $CaBaCo_4O_7$

$CaBaCo_4O_7$ was synthesized from a stoichiometric mixture of CaO, $BaCO_3$ and Co_3O_4 first heated at 900 °C in air during 12 h for decarbonation. The mixture was then pressed in the form of parallelepipedic bars, heated in air at 1100 °C for 12 h, and quenched down to room temperature. The chemical analysis of the sample using iodometric titration showed that the oxygen stoichiometry is "$O_{7.02}$," i.e. the Co^{3+}/Co^{2+} ratio is equal to 1.0 and the energy dispersive spectroscopy (EDS) analysis confirmed that the cationic composition "$Ca_{1.01}Ba_{0.99}Co_{4.02}$" is in agreement with the nominal one, in the limit of the experimental errors.

2.2. Structural and chemical characterization

X-Ray Powder Diffraction (XRPD) patterns were collected using a Panalytical X'Pert Pro diffractometer using Cu $K\alpha$ ($\lambda = 1.5406$ Å) between 7° and 120° (2θ) with a step of 0.0167° at room temperature. Rietveld refinement using FullProf [16] was performed on the pristine and oxidized phases.

Iodometric titrations were performed to determine the cobalt oxidation state in the prepared phases. For iodometric titrations, the end-point was electrochemically determined by following the potential of the solution with platinum electrodes versus ECS electrode, while the current was held at zero. The sample (ca. 50 mg) was dissolved in a 1 M acetic buffer solution (ca. 50 ml) containing an excess of KI (ca.1 g). Co^{+III} and peroxide species were reduced together with formation of iodine species in stoichiometric amount:

$$2Co^{3+} + 3I^- \rightarrow 2Co^{2+} + I_3^-$$

$$H_2O_2 + 3I^- + 2H^+ \rightarrow I_3^- + 2H_2O$$

Iodine was therefore titrated with $Na_2S_2O_3$ 0.1 N solution using thiodene (starch) as colorimetric indicator in addition to the potential evolution

$$2S_2O_3^{2-} + I_2 \rightarrow 2I^- + S_4O_6^{2-}$$

Reproducibility for δ in parallel experiments is ± 0.05.

The electrochemical tests were carried out using a VMP II system (Biologic S.A., Claix) that can be operated in both potentiodynamic and galvanostatic modes. All potential values in this paper are given versus HgO/Hg. Positive electrodes are made with pellets of active material pressed at 2 tons with a mass close to 150 mg. Platinum wire was used as counter electrode in a Tacussel Laboratory test cell and a 1 M KOH solution (from Prolabo, normadose) was used as electrolyte [17].

Electron diffraction (ED) and EDX analysis were performed by using a Tecnai G2 30 UT microscope operated at 300 kV. Jeol 4000 EX microscope operated at 400 kV and having point resolution 0.17 nm was used for high-resolution transmission electron microscopy (HRTEM) analysis. For the transmission electron microscopy (TEM) study, the samples were crushed in methanol and deposited on a holey carbon copper grid. MacTempas and CrystalKit software have been used for image simulations. The dc magnetization measurements were performed by means of a SQUID Quantum Design magnetometer. The ac susceptibility was measured with a PPMS Quantum design with $H_{dc} = 0$ Oe and $H_{ac} = 10$ Oe.

Neutron diffraction experiment was carried out at the D2b diffractometer (ILL, Grenoble) with a wavelength of 1.594 Å.

3. Results and discussion

3.1. Oxidation of $CaBaCo_4O_7$: synthesis of hexagonal $CaBaCo_4O_{7.5}$

Due to the thermal instability of $CaBaCo_4O_7$, and its decomposition into $CaCo_2O_4$, Co_3O_4, $BaCoO_{2.6}$ and $BaCoO_3$ starting at 450 °C in an oxygen flow, the oxidation through oxygen annealing was revealed to be impossible. Thus, we decided to investigate the possible oxygen up-take in such a unique structure by soft chemistry route, either chemically by means of sodium hypochlorite or electrochemically in alkaline medium.

The voltametric polarization curve registered in the 0.0–0.8 V potential window, with a velocity of 275 mV/h (Fig. 1), shows the existence of three domains. Domain I corresponds to the double layers charge of the electrode-electrolyte interface. The wave which lies in the 0.1–0.7 V range (domain II) indicates that $CaBaCo_4O_7$ is oxidized, reaching the composition $CaBaCo_4O_{7.50}$ according to the reaction:

$$CaBaCo_4O_7 + OH^- \leftrightarrow CaBaCo_4O_{7.50} + 0.5H_2O + e^- \quad (1)$$

Finally beyond 0.7 V, the electrolyte oxidation takes place leading to oxygen generation (domain III):

$$4OH^- \rightarrow O_2 + 2H_2O + 4e^- \quad (2)$$

Based on these results, we tried to synthesize the oxidized phase $CaBaCo_4O_{7.50}$, using sodium hypochlorite as oxidizing agent, as previously made for cobalt and nickel oxides [17]. The chemical oxidation of $CaBaCo_4O_7$ was then carried out by placing 0.5 g of this oxide in an aqueous solution of 200 ml of NaClO (13% chlorine active), for 4 days. The sample was then washed with water, filtered and finally dried in an oven at 60 °C. The combined X-ray diffraction and chemical analysis using iodometric titration showed that a pure phase $CaBaCo_4O_{7.50}$ was synthesized according to the reaction equation (3):

$$CaBaCo_4O_7 + 0.5NaOCl \rightarrow CaBaCo_4O_{7.50} + 0.5NaCl \quad (3)$$

3.2. Structural characterization of $CaBaCo_4O_{7.50}$

The structural behavior of $CaBaCo_4O_{7.50}$ is quite unexpected, as shown from its XRPD pattern registered at room temperature (Fig. 2c). The latter reveals its hexagonal symmetry and a small orthorhombic distortion, like that of $YBaCo_4O_7$ (Fig. 2b), is excluded

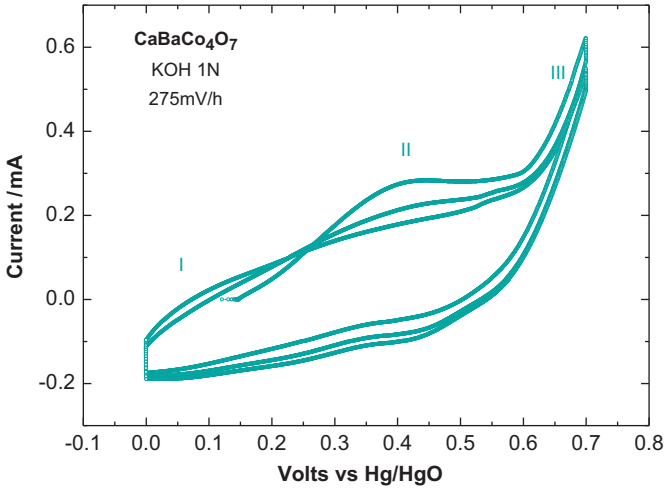

Fig. 1. Cyclic voltammograms on $CaBaCo_4O_7$ working electrode in 1 mol/L KOH solution at 10 mV/s scan rate.

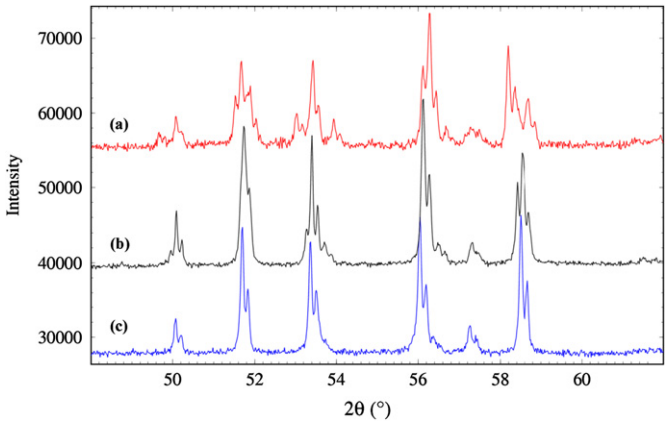

Fig. 2. Part of X-ray diffraction patterns for: (a) $CaBaCo_4O_7$, (b) $YBaCo_4O_7$ and (c) $CaBaCo_4O_{7.5}$. The splitting of some reflections in $CaBaCo_4O_7$ and $YBaCo_4O_7$ reflects their orthorhombic symmetry, while $CaBaCo_4O_{7.5}$ has the hexagonal symmetry.

by the sharpness of the diffraction peaks. Thus, staring from the distorted orthorhombic $CaBaCo_4O_7$ phase (Fig. 2a), the introduction of extra oxygen leads paradoxally to higher symmetry. This hexagonal symmetry, compatible with the space groups $P6_3mc$ or $P31c$ is also confirmed by its neutron powder diffraction (NPD) pattern (not shown). All the diffraction peaks can be indexed to a hexagonal cell with the following parameters: $a_H = 6.3074(1)$ Å and $c_H = 10.2565(2)$ Å.

The electron microscopy investigations confirm without any ambiguity the different symmetry of $CaBaCo_4O_{7.50}$ compared to $CaBaCo_4O_7$. The ED patterns of $CaBaCo_4O_7$ collected from the main zone axis (Fig. 3) before oxidation are clearly indexed in the orthorhombic space group $Pna2_1$ (a = 11.00 Å, b = 6.29 Å, c = 10.19 Å), as previously reported [9,10], whereas the oxidized $CaBaCo_4O_{7.50}$ sample shows two sorts of microcrystals, in rather equivalent amounts. The first type of crystals exhibit reflection conditions, characteristic of the hexagonal ($P6_3mc$) or trigonal ($P31c$) symmetry with $a_H \sim 6.31$ Å and $c_H \sim 10.26$ Å previously observed for $YBaCo_4O_7$ above 310 K [6], as shown from their [0 0 0 1] and [2 $\bar{1}$ $\bar{1}$ 0] ED patterns (Fig. 4a, b). The second type of crystals show similar ED patterns (Fig.4c, d) except for the [0 0 0 1] zone axis. Indeed, the [0 0 0 1] ED patterns exhibit, besides basic hexagonal strong spots, additional weak superstructure spots (Fig.4c). The appearance of such superstructure spots corresponds to the hexagonal supercell, $a_{HS} \approx a_H\sqrt{3}$. The intensities of these superstructure spots are not equivalent and clearly point out the double diffracted spots, which were confirmed by tilting experiment along relevant axis. The reflection conditions of this new supercell are compatible with the hexagonal space group $P6_3cm$ (1 8 5) with $a_{HS} \sim 10.92$ Å and $c_{HS} \sim 10.26$ Å. It is important to point out that after a rather short exposure to the electron beam (few seconds) the superstructure reflections have almost disappeared (Fig. 5), leading to the basic hexagonal cell shown in Fig. 4a. The weak intensity and fast degradation of the superstructure spots under e-beam suggest a possible induced disordering.

Based on these observations, attempts were made to solve the structure of this new hexagonal form of $CaBaCo_4O_{7.50}$ from XRPD and NPD data, starting from the atomic positions previously obtained for $YbBaCo_4O_7$ [5]. Bearing in mind that the close packed nature of this hexagonal structure should not allow extra oxygen to be inserted with respect to the ideal composition $CaBaCo_4O_7$, two structural hypotheses were considered, successively, that we call "cationic deficiency" and "quasi peroxo groups" scenario. Important to notice, that the EDX analysis of number of crystals before ($CaBaCo_4O_7$) and after oxidation ($CaBaCo_4O_{7.5}$) shows the Ca/Ba ratio remains the same, being close to the nominal composition.

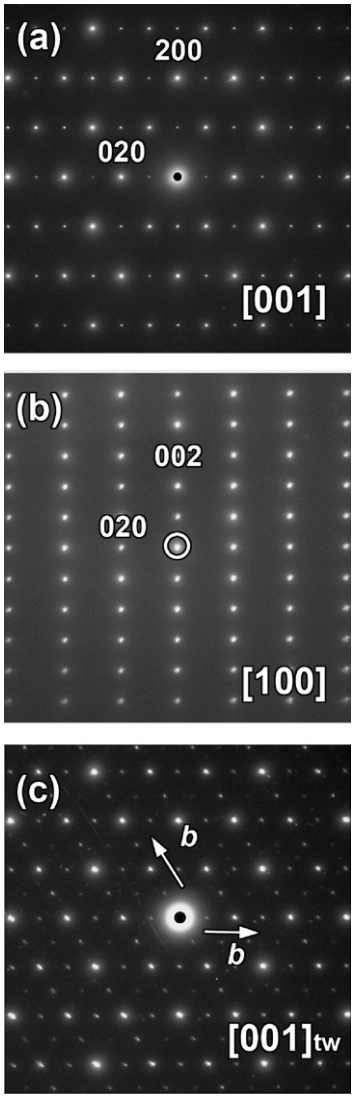

Fig. 3. (a, b) Electron diffraction patterns of $CaBaCo_4O_7$ along main zone axis and (c) [0 0 0 1] ED pattern of 60° rotated twin region.

The cationic deficiency scenario is based on the fact that the oxidation of orthorhombic $CaBaCo_4O_7$ to hexagonal $CaBaCo_4O_{7.50}$, which takes place at room temperature, is most probably topotactic, suggesting that the "barium oxygen" framework remains close packed. Such an oxidation reaction would be similar to that observed for the oxidation of the spinels Fe_3O_4 and Co_3O_4 into γ-Fe_2O_3 and $Co_{3-x}O_4$ oxides, respectively, which do not contain interstitial oxygen , but were found to be iron or cobalt deficient spinels [18,19]. The close relationships between the spinel and the "114" hexagonal structures also support this hypothesis. Consequently, according to this model the oxidation of $CaBaCo_4O_7$ to $CaBaCo_4O_{7.50}$ should correspond to the reaction:

$$0.94CaBaCo_4O_7 + 0.24O_2 \rightarrow Ca_{0.94}(Ba_{0.94}O_{0.06})Co_{3.76}O_7$$

The "quasi peroxo groups" scenario, deals with the possible partial replacement of single oxygen ion O^{2-} by peroxo groups $(O_2)^{2-}$, leading to short O–O distances in the "peroxo" groups (1.48 Å), similar to BaO_2 [20] but correct interatomic distances for the rest of the structure. The presence of such groups in oxides is rare, but not exceptional and was observed in the hydrated tungsten peroxide $[WO_2(O_2)H_2O].nH_2O$ [21] and in the ruthenium oxide $Ba_5Ru_2O_9(O_2)$ [22]. A preliminary refinement of the structure from NPD data in the $P6_3cm$ classical space group, previously

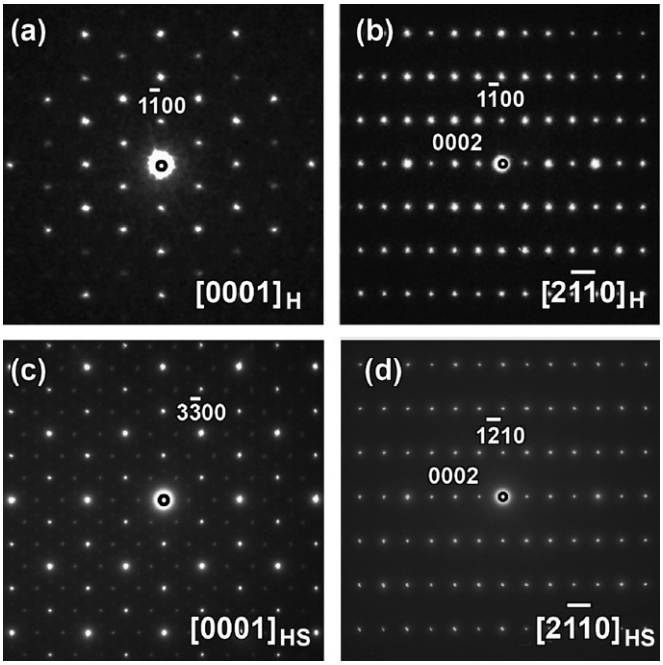

Fig. 4. Electron diffraction patterns of $CaBaCo_4O_{7.5}$ along main zone axis for basic hexagonal structure (a) $[0\,0\,0\,1]_H$, (b) $[2\,\text{-}1\,\text{-}1\,0]_H$ and modulated hexagonal structure (c) $[0\,0\,0\,1]_{HS}$ and (d) $[2\,\text{-}1\,\text{-}1\,0]_{HS}$.

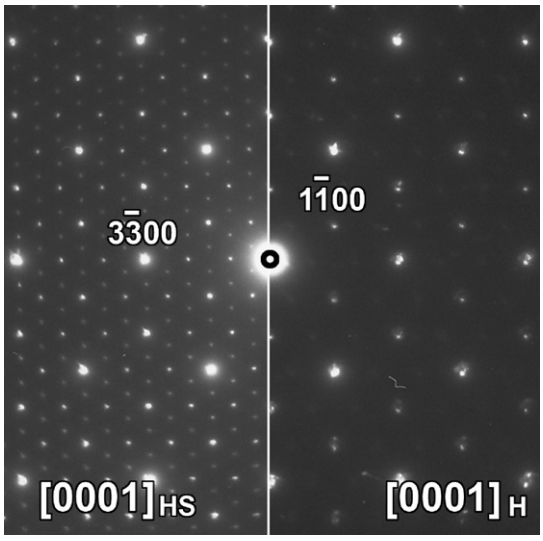

Fig. 5. $[0\,0\,0\,1]_{HS}$ $CaBaCo_4O_{7.5}$ ED patterns taken immediately (left half) and after approximately 1 min (right half). Notice the disappearance of superstructure spots after short time irradiation.

observed for $YbBaCo_4O_7$ [5] led to atomic positions similar to those of this compound, but the agreement factors remain high ($R_{bragg} \sim 0.1$) and the excess oxygen could not be located from the data. Then starting from the above "stoichiometric" model attempts to refine the occupancy factors of oxygen, of cobalt and barium sites successively were unsuccessful leaving the *R* factors practically unchanged for the NPD and for the XRD data. In the last step, introduction of additional oxygen in the "00z" and "00z+d" positions, to mimic the peroxide ions was considered. No improvement of the *R* factors was obtained from NPD data. Finally, *ab initio* structure calculations were carried but they lead to the initial unsatisfactory solution, without any possibility to detect the oxygen excess or cation deficiency. Thus, the issue of the location of extra oxygen in $CaBaCo_4O_{7.5}$ is still pending.

Nevertheless, it is worth to emphasize that the comparative HRTEM study of $CaBaCo_4O_7$ and $CaBaCo_4O_{7.50}$ reveals that the two structures are very closely related. In the HRTEM images along [0 0 1] and [1 0 0] zone axis of orthorhombic $CaBaCo_4O_7$ structure (Fig. 6a and b, respectively), the brightest rows of dots correspond to projection of Ba columns. The [0 0 0 1] zone of hexagonal $CaBaCo_4O_{7.50}$ (Fig. 7a) is similar to that previously observed for $YBaCo_4O_7$ cobaltites. The [2 -1 -1 0] HRTEM image of $CaBaCo_4O_{7.50}$ (Fig. 7b) and [1 0 0] of $CaBaCo_4O_7$ show a perfect crystal structure along *c*-axis for both structures, which is free of any defect, stacking faults or disorder along the *c*-axis. Note that HRTEM images of the second form of $CaBaCo_4O_{7.50}$ characterized by superstructure spots (Fig.4c) could not be recorded, due to instability of the superstructure under the electron beam as is shown in Fig. 5.

3.3. Magnetic properties of $CaBaCo_4O_{7.50}$

The temperature dependence of the dc magnetization, which was registered according to the standard zero-field-cooled (ZFC) and field-cooled (FC) procedures (under a magnetic field of 0.3 T), is shown in Fig. 8. A large thermomagnetic irreversibility is seen in

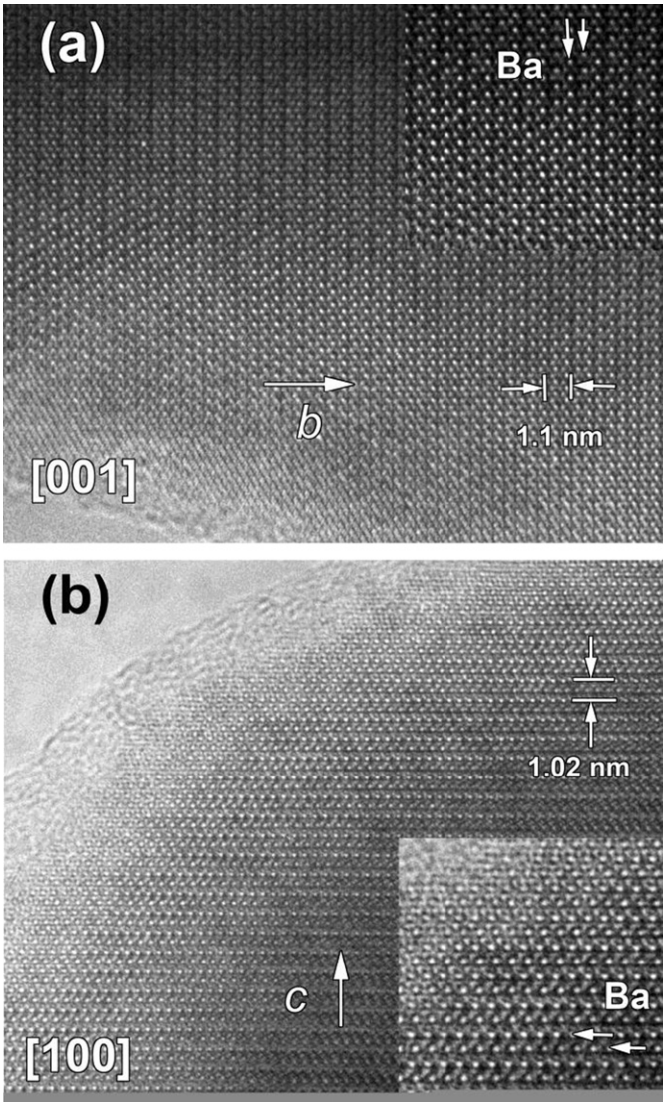

Fig. 6. HRTEM image of $CaBaCo_4O_7$ along the [0 0 1] (a) and [1 0 0] (b) zone axis. The brightest dots represent Ba columns marked by white arrows in enlargement image given as insert.

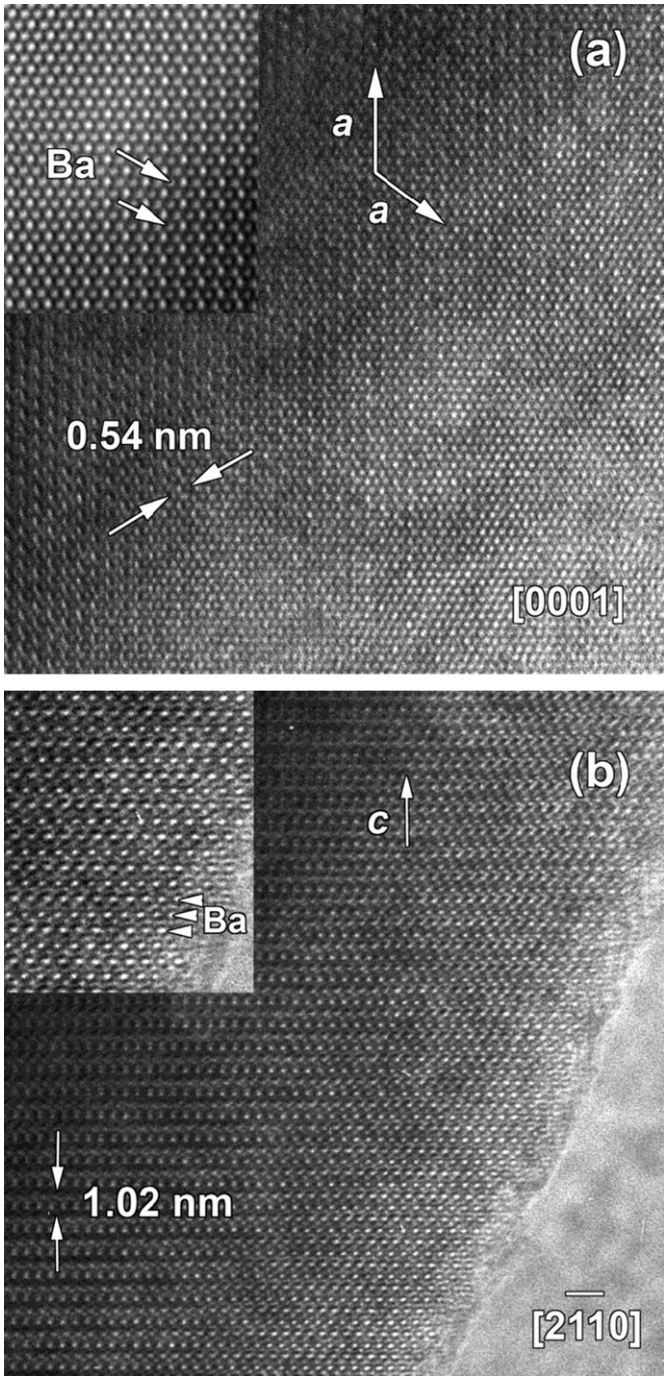

Fig. 7. HRTEM image of $CaBaCo_4O_{7.5}$ along the [0 0 1] (a) and [1 0 0] (b) zone axis. The brightest dots represent Ba columns marked by white arrows in enlargement image given as insert.

the temperature dependence of magnetization. In the zero-field-cooled condition, the magnetization initially increases as the temperature is increased, reaches a maximum at $T_{max}=45$ K, and then starts decreasing with increasing temperature. In the field-cooled condition, M_{FC} decreases continuously with increasing temperature. Such a large irreversibility in the ZFC and FC magnetization behavior is seen either in spin glass systems, or in ordered systems with large magnetocrystalline anisotropy. In our sample, we can safely rule out magnetic frustration and spin glass behavior because the ac magnetic susceptibility measurements (shown later) reveal a frequency independent peak in both the real as well as imaginary parts. Thus, $CaBaCo_4O_{7.5}$ is an anisotropic

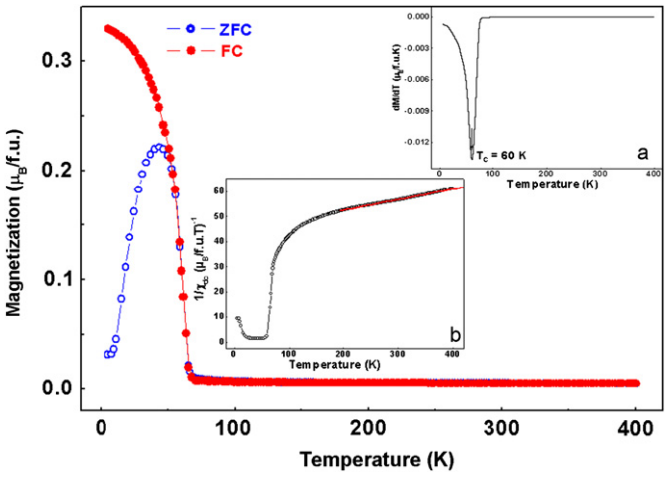

Fig. 8. $M_{ZFC}(T)$ and $M_{FC}(T)$ curves for $CaBaCo_4O_{7.5}$ measured at $H=0.3$ T. Inset (a) shows the dM/dT vs. T curve and inset (b) shows the $\chi^{-1}(T)$ curve. (For interpretation of the references to colour in this figure, the reader is referred to the web version of this article.)

material. The sample undergoes a para to ferro (or ferri) magnetic transition at $T_C=60$ K (estimated from the inflection point of the dM/dT versus T curve, shown in inset (a) of Fig. 8). Below T_C, magnetic anisotropy aligns the spins in a preferred direction. Since no magnetic field is applied while cooling the sample through the ordering temperature during the process of zero-field cooling, the spins get locked in random directions. When a magnetic field is applied at the lowest temperature, far below the Curie temperature, the magnitude of the resultant magnetization depends on the anisotropy of the system. If the system is highly anisotropic (i.e. the anisotropy field is larger than the applied field), then the applied field will not be sufficient to rotate the spins in the direction of the applied field, and the magnetization will be very small. This is what happened in our case. During the field-cooled process, the sample is cooled through its Curie temperature in presence of a magnetic field. Therefore, the spins will be locked in a particular direction as soon as the system is cooled below its ordering temperature. For highly anisotropic materials, the FC magnetization will increase continuously with decreasing temperature (as is seen for our sample). In inset (b) of Fig. 8, we have shown the $\chi^{-1}(T)$ curve of this compound. A linear fit of the high temperature region (shown by a red line in the figure) yields a very large negative Curie–Weiss constant ($\theta_{CW}=-1043$ K), and a magnetic moment of 4.86 μ_B per Co.

Fig. 9 shows the unusual magnetic hysteresis behavior of this oxide. The data have been recorded at 5 K. The initial magnetization curve is S-shaped, and the anisotropy field ($H_{anisotropy}=1.37$ T, as marked in the inset of Fig. 9) is much larger than the coercive field ($H_C=0.16$ T). The magnetization increases very slowly with increasing fields for $H<H_{anisotropy}$, indicating that there is considerable resistance to the domain wall motion at low fields. The virgin curve lies outside the hysteresis loop above H_C, and meets the main loop only at very high fields. This unusual magnetic hysteresis behavior may be associated with irreversible domain wall motion; possibly arising from defect induced pinning.

This irreversible behavior decreases rapidly as the temperature increases (Fig. 10) and finally disappears close to $T_C\sim60$ K.

The temperature evolution of the real part $\chi'(T)$ and imaginary part $\chi''(T)$ of the magnetic susceptibility at two different frequencies, 10 Hz and 10 kHz (Fig.11) shows a peak at 60 K, which corresponds to the paramagnetic to ferrimagnetic transition in this sample. The fact that the position of the peak does not shift even under a frequency change of 3 decades confirms the absence of magnetic frustration in this sample.

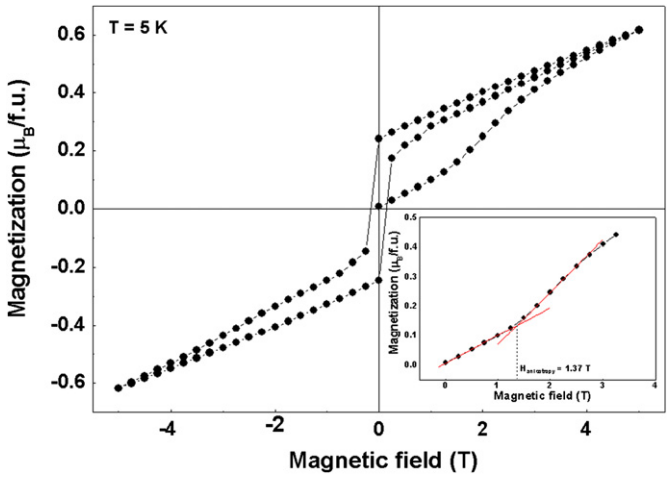

Fig. 9. $M(H)$ curve for $CaBaCo_4O_{7.5}$ at $T=5$ K. The inset shows the initial part of the virgin curve indicating the anisotropy field, $H_{anisotropy}$.

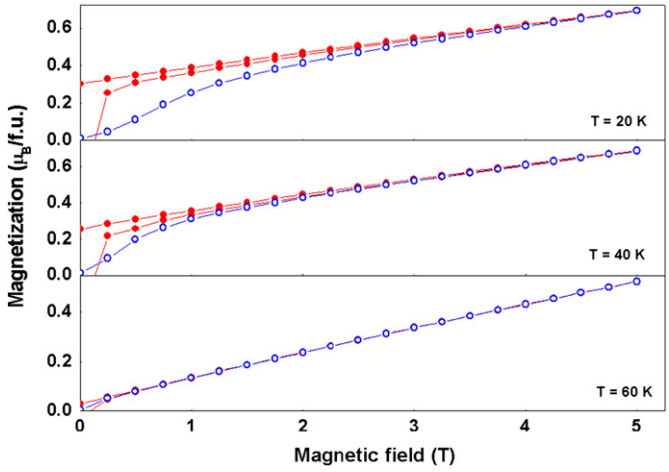

Fig. 10. Initial magnetization (blue open circles) and part of the hysteresis loop (red closed circles) of $CaBaCo_4O_{7.5}$ measured at 20 K, 40 K and 60 K. (For interpretation of the references to colour in this figure legend, the reader is referred to the web version of this article.)

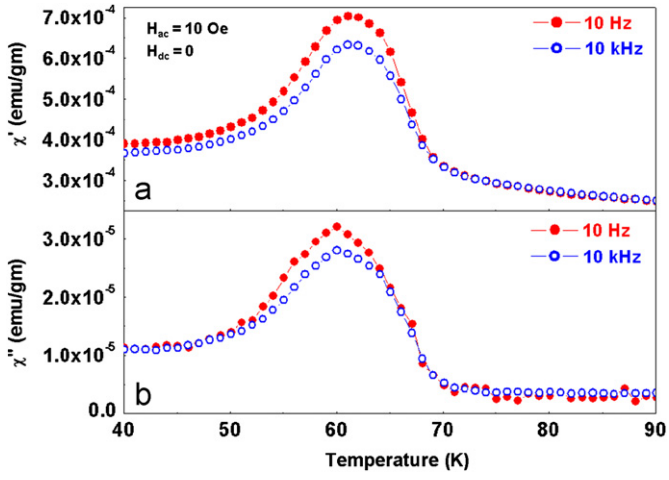

Fig. 11. (a) Real (in-phase) and (b) imaginary (out-of-phase) component of ac susceptibility for $CaBaCo_4O_{7.5}$ as a function of temperature.

The fact that $CaBaCo_4O_{7.50}$ is, like $CaBaCo_4O_7$, ferrimagnetic and exhibits an identical T_C value is remarkable. It shows that the hexagonal symmetry of this phase does not induce an important magnetic frustration in contrast to $YBaCo_4O_7$, which has been shown to exhibit a strong competition between 1D magnetic ordering along c and 2D magnetic frustration in the (0 0 1) plane [8]. This different behavior may be due to the defects introduced by the oxidation, which modify the local environment of cobalt and consequently influence the crystal field significantly. Thus, it is most probable that these defects play the role of pinning centers, explaining the unusual magnetic hysteresis loops observed for this phase.

4. Conclusion

This study shows the extraordinary ability of the "114" cobaltite $CaBaCo_4O_7$ to absorb oxygen topotactically, in spite of the close packed character of its structure. Remarkably, the oxidation of $CaBaCo_4O_7$ brings about a structural transition from the orthorhombic to hexagonal symmetry, raising the issue of the location of extra oxygen in such a close packed structure. The magnetic properties of $CaBaCo_4O_{7.5}$, compared to those of $CaBaCo_4O_7$, are also of great interest, showing that the oxidized phase remains ferrimagnetic with the same T_C as the pristine phase, but with an unusual magnetic hysteresis behavior characteristic of considerable resistance domains wall motion. The absence in this oxide of 2D magnetic frustration, in contrast to the $YBaCo_4O_7$ family which exhibits the same hexagonal symmetry is also quite remarkable. All these results open the route for understanding the mechanism of oxygen storage, which has been studied on the very similar $LnBaCo_4O_{7+\delta}$ cobaltites.

Acknowledgments

The authors are very grateful to Prof. G. Van Tendeloo for allowing the HRTEM micrographs to be taken at EMAT, University Antwerpen by one of us (O. I. L.). We also gratefully acknowledge the CNRS and the Minister of Education and Research for financial support through their Research, Strategic, and Scholarship programs (ANR-09-JCJC-0017 "TUNE", JC09_442369), and the European Union for support through the network of excellence Novelox and FAME. T. S. acknowledges the Conseil Regional of Basse Normandie for financial support in the frame of Emergence Program.

References

[1] D.V. Sheptyakov, A. Podlesnyak, S.N. Barilo, S.V. Shiryaev, D.D. Khalyavin, D.Yu Chernyshov, L.I. Leonyuk, PSI Sci. Rep. 3 (2001) 64.
[2] M. Valldor, M. Andersson, Solid State Sci. 4 (2002) 923.
[3] V. Caignaert, A.M. Abukumov, D. Pelloquin, V. Pralong, A. Maignan, G. Van Tendeloo, B. Raveau, Chem. Mater. 21 (2009) 1116;
V. Pralong, V. Caignaert, A. Maignan, B. Raveau, J. Mater. Chem. 19 (2009) 8335.
[4] L.C. Chapon, P.G. Radaelli, H. Zheng, J.F. Mitchell, Phys. Rev. B 74 (2006) 172401.
[5] A. Huq, J.F. Mitchell, H. Zheng, L.C. Chapon, P.G. Radaelli, K.S. Knight, P.W. Stephens, J Solid State Chem. 179 (2006) 1136.
[6] V. Caignaert, A. Maignan, V. Pralong, S. Hébert, D. Pelloquin, Solid State Sci. 8 (2006) 1160;
A. Maignan, V. Caignaert, D. Pelloquin, S. Hebert, V. Pralong, J. Hejtmanek, D. Khomskii, Phys. Rev. B 74 (2006) 165110.
[7] M. Valldor, J. Phys. Condens. Matter 16 (2004) 9209.
[8] P. Manuel, L.C. Chapon, P.G. Radaelli, H. Zheng, J.F. Mitchell, Phys. Rev. Lett. 103 (2009) 037202.
[9] V. Caignaert, V. Pralong, A. Maignan, B. Raveau, Solid State Commun. 149 (2009) 453.
[10] V. Caignaert, V. Pralong, V. Hardy, C. Ritter, B. Raveau, Phys. Rev. B 81 (2010) 094417.
[11] M. Karppinen, H. Yamauchi, S. Otani, T. Fujita, T. Motohashi, Y.H. Huang, M. Vakeapaa, H. Fjellvag, Chem. Mater. 18 (2006) 490.
[12] E.V. Tsipis, D.D. Khalyavin, S.V. Shirayev, K.S. Redkina, P. Nunez, Mater. Chem. Phys. 92 (2005) 33.
[13] S. Kadota, M. Karpinnen, T. Motohashi, H. Yamauchi, Chem. Mater. 20 (2008) 6378.

[14] O. Chmaissem, H. Zheng, A. Huq, P.W. Stephens, J.F. Mitchell, J. Solid State Chem. 181 (2008) 664.
[15] Y. Jia, H. Jiang, M. Valkeapaa, H. Yamauchi, M. Karppinen, E.I. Kauppinen, J. Am. Chem. Soc. 131 (2009) 4880.
[16] J. Rodriguez-Carvajal, Physica B 192 (1993) 55.
[17] V. Pralong, A. Delahaye-Vidal, B. Beaudoin, B. Gérard, J-M. Tarascon, J. Mater. Chem. 9 (1999) 950;
V. Pralong, A. Delahaye-Vidal, Y. Chabre, B. Beaudoin, J-M. Tarascon, J. Solid State Chem. 162 (2001) 270.
[18] J.E. Jorgensen, L. Mosegaard, L.E. Thomsen, T.R. Jensen, J.C. Hanson, J. Solid State Chem. 180 (2007) 185.
[19] M. Douin, L. Guerlou-Demourgues, M. Menetrier, E. Bekaert, L. Goubault, P. Bernard, D. Delmas, J. Solid State Chem. 182 (2009) 1273.
[20] J.D. Bernal, E. Djatlowa, P. Kasarnowsky, S. Reichstein, A.G. Ward, Z. Kristallogr. 92 (1935) 344.
[21] B. Pecquenard, S. Castro-Garcia, J. Livage, P.Y. Zavalij, M.S. Whittingham, R. Thouvenot, Chem. Mater. 10 (1882) (1998).
[22] F. Grasset, C. Dussarrat, J. Darriet, J. Mater. Chem. (7, 1911) 1997.